Rare Met. (2022) 41(11):3630–3638
https://doi.org/10.1007/s12598-022-02066-2

RARE METALS

LETTER

In situ construction of a favorable cathode electrolyte interphase through a fluorosilane additive for high-performance Li-rich cathode materials

Yuan-Yuan Pan, Chang-Ding Qiu, Shi-Jie Qin, Zuo-Fei Wang, Jing-Song Yang, Heng-Jiang Cong, Fu-Sheng Ke*

Received: 6 April 2022 / Revised: 24 April 2022 / Accepted: 25 April 2022 / Published online: 16 August 2022

Li-rich manganese-based oxides (LRMO) with high capacities are attractive cathode materials for next-generation lithium-ion batteries. However, poor cycling stability is one of the key issues impeding their commercialization. Here, for the first time, we employed trimethoxy(3,3,3-trifluoropropyl)silane (TMTFS) as a multifunctional electrolyte additive to stabilize the LRMO cathode interphase and elevate its cycling performance. The LRMO electrode delivered a high reversible capacity of 250.4 $mAh{\cdot}g^{-1}$ with a stable capacity retention of 91% after 200 cycles. Detailed analysis using in situ powder X-ray diffraction (PXRD), cyclic voltammetry (CV), nuclear magnetic resonance (NMR), X-ray photoelectron energy spectra (XPS) and transmission electron microscopy (TEM) demonstrated that the TMTFS additive can not only form a robust, thin, and dense LiF-dominated cathode electrolyte interphase, but also scavenge detrimental HF in electrolyte. Additionally, the TMTFS additive can adjust the solvation environment, thus enhancing the transference number of lithium ions.

With the explosively growing demand of portable electronic devices and pure/hybrid electric vehicles, it is urgent to develop rechargeable lithium-ion batteries (LIBs) with high energy and high power densities [1]. Compared to anode materials, the energy density of commercial LIBs has reached a bottleneck, which is limited by the cathode materials [2–5]. The mainly commercial cathode materials have lower capacities, such as $LiCoO_2$ (140 $mAh{\cdot}g^{-1}$) [6] and $LiFePO_4$ (150 $mAh{\cdot}g^{-1}$) [7, 8]. Therefore, it is crucial to seek or optimize cathode materials with high capacity for next-generation LIBs.

Among the high capacity cathode materials, Li-rich manganese-based oxides (LRMO), a formula of $xLiMO_2{\cdot}(1-x)Li_2MnO_3$ or $Li_{1+x}M_{1-x}O_2$ ($0 < x < 1$, M = Ni, Co, Mn), have attracted considerable attention on high theoretical capacities (> 300 $mAh{\cdot}g^{-1}$) and a wide voltage range of 2.0–4.8 V (vs. Li/Li^+), compared with Ni-rich NCM (lithium nickel cobalt manganese oxide) and NCA (lithium nickel cobalt aluminum oxide) [9–11]. However, the LRMO materials usually have a large initial capacity loss [12, 13], poor rate capability [14, 15], fast capacity decay and continuous voltage fading upon cycling [16–18], which seriously hinders them for the practical LIBs applications. Various studies demonstrated that the poor electrochemical performance of LRMO materials originates from the following: (1) the irreversible oxidation of O^{2-} occurred once charged to 4.4–4.8 V (vs. Li/Li^+), resulting in a low initial Coulombic efficiency (ICE) [12, 18]; (2) the irreversible oxygen release induced oxygen vacancy and transition-metal ions migration into Li layer, leading to voltage fading and capacity degrading [19–21]; (3) the continuous high voltage interfacial side reactions and the dissolution of transition-metal ions in electrolyte under the corrosion of hydrofluoric acid, resulting in thick cathode electrolyte interphase (CEI) layer and poor rate capability [22, 23], respectively.

To solve/mitigate the above detrimental effects, several strategies have been reported. One strategy focuses on the

Supplementary Information The online version contains supplementary material available at https://doi.org/10.1007/s12598-022-02066-2.

Y.-Y. Pan, C.-D. Qiu, S.-J. Qin, Z.-F. Wang, J.-S. Yang, H.-J. Cong, F.-S. Ke*
Sauvage Center for Molecular Sciences, College of Chemistry and Molecular Sciences, Wuhan University, Wuhan 430072, China
e-mail: kefs@whu.edu.cn

cathode materials, such as surface modification [24, 25], cation or anion doping [14, 26, 27]. One typical example is coating Li_3PO_4 with high ionic conductivity and the substances with high electronic conductivity on the surface of high-capacity layered oxide cathode materials, resulting in restraining the interfacial side reactions, and promoting the ionic and electronic conductivity [24, 28–31]. Recently, Wynn and co-workers [32] demonstrated that the Mo-doped LRMO tuned charge density distribution and the local band structure to enhance the electrochemical performances. Another strategy focuses on the electrode construction, i.e., introducing functional binder or conductivity to build the electrode [33, 34]. Various binders, such as sodium carboxymethyl cellulose (CMC) and polyacrylic acid (PAA), were employed to construct the stable electrodes, which indicated that the voltage-fading phenomena were alleviated [17, 35]. The third strategy focuses on the electrolyte, for instance, adding new solvents or additives [36–38]. Meng and co-workers used LiBOB as an additive, which can remove HF and form stable CEI layer, resulting in relieving particles' surface/subsurface phase transformation and alleviating voltage decay [39]. Similar study was also carried out by Zhang et al. [23]. Compared to the above three strategies, adding electrolyte additive is an easier approach, which can be accepted by the battery manufacturers.

In this study, we are the first to choose TMTFS as a functional electrolyte additive. The electrochemical performance of this additive displayed higher cycling stability of LRMO electrodes. In situ PXRD, NMR, XPS and TEM revealed the TMTFS additive to form a thin and uniform LiF-enriched CEI layer, which effectively protected the LRMO particles during the cycling. The TMTFS additive tuned the solvation environment of lithium ions, resulting in enhancing Li-ion transference number and inhibiting the decompose of PF_6^-. Meanwhile, it can also effectively scavenge hydrogen fluoride (HF), which can corrode the LRMO structure, from the electrolyte.

The LRMO ($Li_{1.2}Ni_{0.13}Co_{0.13}Mn_{0.54}O_2$) material was synthesized by a simple polymer-pyrolysis method [17, 40–42]. The structure and morphology of the as-synthesized LRMO were characterized by PXRD, SEM and TEM, as shown in Fig. 1. PXRD pattern of the LRMO has a typical layered hexagonal structure of α-$NaFeO_2$ lattice with space group of $R\bar{3}m$ (Fig. 1a). Meanwhile, the peaks from 20° to 25° belonged to the formation of Li_2MnO_3, which were referred to as superlattice reflections [43]. It was worth noting that the clearly split diffraction peaks of (006), (012), (018) and (110) were observed, indicating the sample with a well-layered structure. The ratio of the peak intensity of (003)/(104) in the PXRD pattern corresponds to the cation disorder degree between lithium and transition metal sites [24, 40]. In addition, the particle size of LRMO nanoparticle is about 200–300 nm (Fig. 1b, c). The clear edge and angle were observed in each of particles from SEM image, which confirmed the LRMO nanoparticles with crystal structure. High-resolution transmission electron microscopy (HRTEM) image (Fig. 1d) indicates that the distance between adjacent lattice plane is measured about 0.47 nm, which is in good agreement with the *d*-spacing of the (003) plane of the LRMO.

Coin cells were employed to evaluate electrochemical properties of the LRMO cathode in the LB-372 electrolyte with and without TMTFS additive. Figure 2a presents the initial charge–discharge profiles of LRMO electrodes in LB-372 and LB-372-1.0 vol% TMTFS electrolytes. Both of them exhibit similar charge–discharge behaviors with a considerable discharge capacity of 286.3 and 283.3 $mAh{\cdot}g^{-1}$ for LB-372 and LB-372-1.0 vol% TMTFS electrolytes, respectively. Figures 2b and S1b show the cycle performance of batteries with different electrolytes at 0.4C (1.0C = 250 $mA{\cdot}g^{-1}$). LRMO electrode in the LB-372 electrolyte displayed an initial capacity of 241.1 $mAh{\cdot}g^{-1}$ and the capacity retention of 77% after 200 cycles. While the LRMO cathode in LB-372-1.0 vol% TMTFS electrolyte showed clearly improved stability, which had the first capacity of 250.4 $mAh{\cdot}g^{-1}$, corresponding capacity retention of 91% under identical conditions. When the content of TMTFS additive increased to 2.5 vol% and 5.0 vol% (Fig. S2a), the capacity retention was 89% and 83% after 200 cycles at 0.4C. Additionally, different fluorosilane and n-propyltrimethoxysilane (without fluorine) were chosen as control experiments, as shown in Fig. S2c, d, which demonstrated the TMTFS additive with the best electrochemical performance among them. To further assess the stability at high current densities, we measured the rate dependence of specific capacity of the LRMO cathode in the electrolyte with and without 1.0 vol% TMTFS, as shown in Figs. 2c, S1a–d. When the electrolyte included TMFTFS, the reversible capacities of the electrodes are 195.8 and 162.2 $mAh{\cdot}g^{-1}$ after 200 cycles at 1.0C and 2.0C, respectively. An over-charge phenomenon was observed in the LB-372 electrolyte after over 100 cycles in all current densities (Fig. S1b–d). This phenomenon brought forward to ~ 40th cycle when the charge voltage range extended to 5.0 V (Figs. 2d, S1e). This result illustrated that the LB-372 electrolyte is unstable for the high voltage cathode materials during cycling. Fortunately, the TMTFS additive can improve the stability of electrolyte at high voltage during charge process and overcome this over-charge phenomenon.

To understand why the electrolyte with TMTFS additive exhibits excellent cycling performance, we carried out analysis on the electrolytes and the electrode/electrolyte

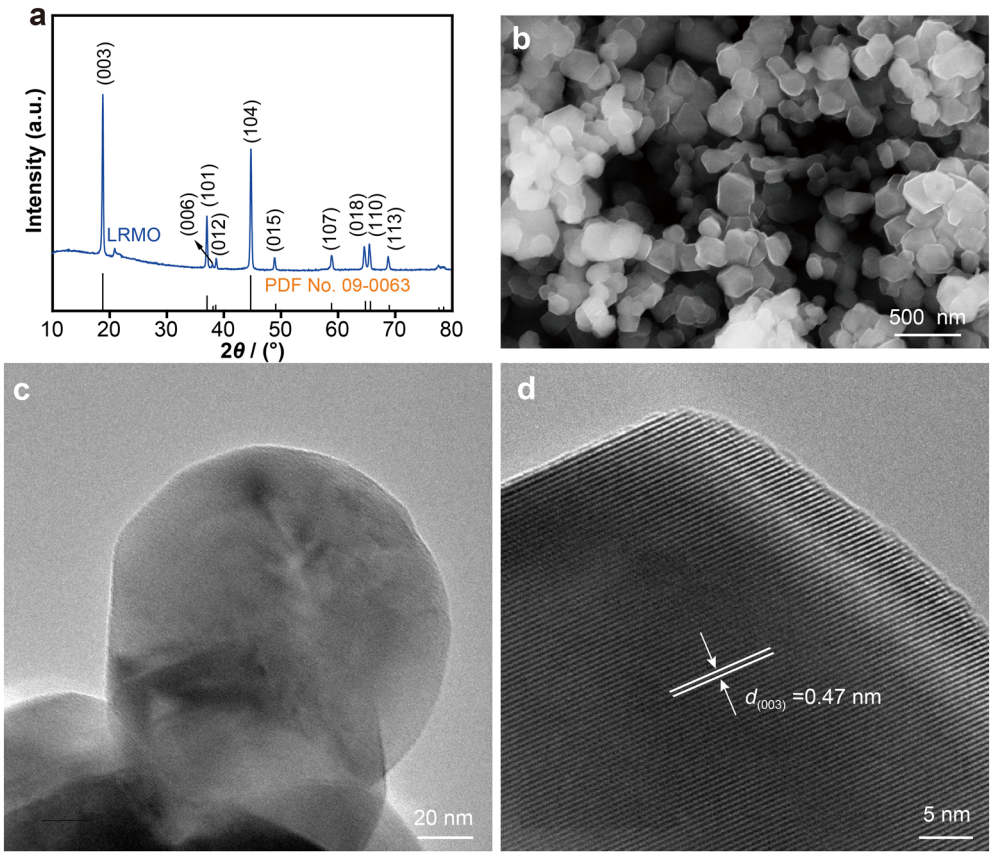

Fig. 1 **a** XRD pattern, **b** SEM image, **c** TEM image and **d** HRTEM image of synthesized $Li_{1.2}Ni_{0.13}Co_{0.13}Mn_{0.54}O_2$ nanocrystals

interface. We first performed NMR measurements on electrolyte with and without TMTFS additive to study the chemical environment of Li and F. When the TMTFS was added into the electrolyte, it could change the solvation structure of Li^+. Upon adding the additive in the LB-372 electrolyte, the ^{7}Li peak shifts downfield (more positive, Fig. 2e), which is indicative of decreased Li^+-solvent interaction, resulting in less electron density around Li^+ [40]. It means that the less solvent molecules are around Li^+, which can move faster in this electrolyte during charge–discharge processes. This result was confirmed by the lithium-ion transference number through the Bruce–Vincent–Evans technique (Fig. S3) [44].

The solute of electrolyte, $LiPF_6$, is a moisture-sensitive component, which is easy decomposed to form HF and $PO_2F_2^-$. HF is a harmful species, resulting in etching the LRMO and current collectors [45, 46]. Therefore, the electrolyte with the function of scavenging HF is one of the strategies to enhance the cycling performance. The ^{19}F NMR spectra of electrolytes are shown in Figs. 2f, S4. When adding HF aqueous solution in LB-372 electrolyte, new peaks belonging to HF (-192×10^{-6}) and $PO_2F_2^-$ (-85×10^{-6} and -87×10^{-6}) were observed. The ^{19}F peak of HF was not detected after adding HF in LB-372 electrolyte with 1.0 vol% TMTFS. Meanwhile, the peak intensity of $PO_2F_2^-$ clearly decreased. It demonstrated that the TMTFS additive not only scavenged HF, but also suppressed the hydrolysis of $LiPF_6$. This result is different with that of (2-allylphenoxy) trimethylsilane additive, which still observed peaks of $PO_2F_2^-$ [47].

Both of the ^{7}Li and ^{19}F NMR spectra revealed that the TMTFS additive can change the structure of electrolyte, and it also will change the interface between cathode and electrolyte. HRTEM, XPS, electrochemical impedance spectroscopy (EIS) and CV were employed to analyze and characterize the electrode/electrolyte interface. Firstly, the LRMO particles after charge–discharge cycles in both electrolytes were characterized through TEM, as shown in Fig. 3a, b. A roughness layer, with thickness from nanometers to 25 nm, was observed on the LRMO particle in LB-372 electrolyte. It seems to be etched by HF, which is from hydrolysis of $LiPF_6$ or the decomposition of the electrolyte under high potential. Such thick and unshaped interphase layer may hinder the transportation of Li^+ between electrolyte and LRMO particles. In contrast, the surface of the LRMO particles has a uniform and smooth layer when adding TMTFS into the electrolyte. The thickness of the interphase layer is about 4 nm. Compared to both TEM images (Fig. 3a, b), they confirmed that the TMTFS affected the electrode/electrolyte interface.

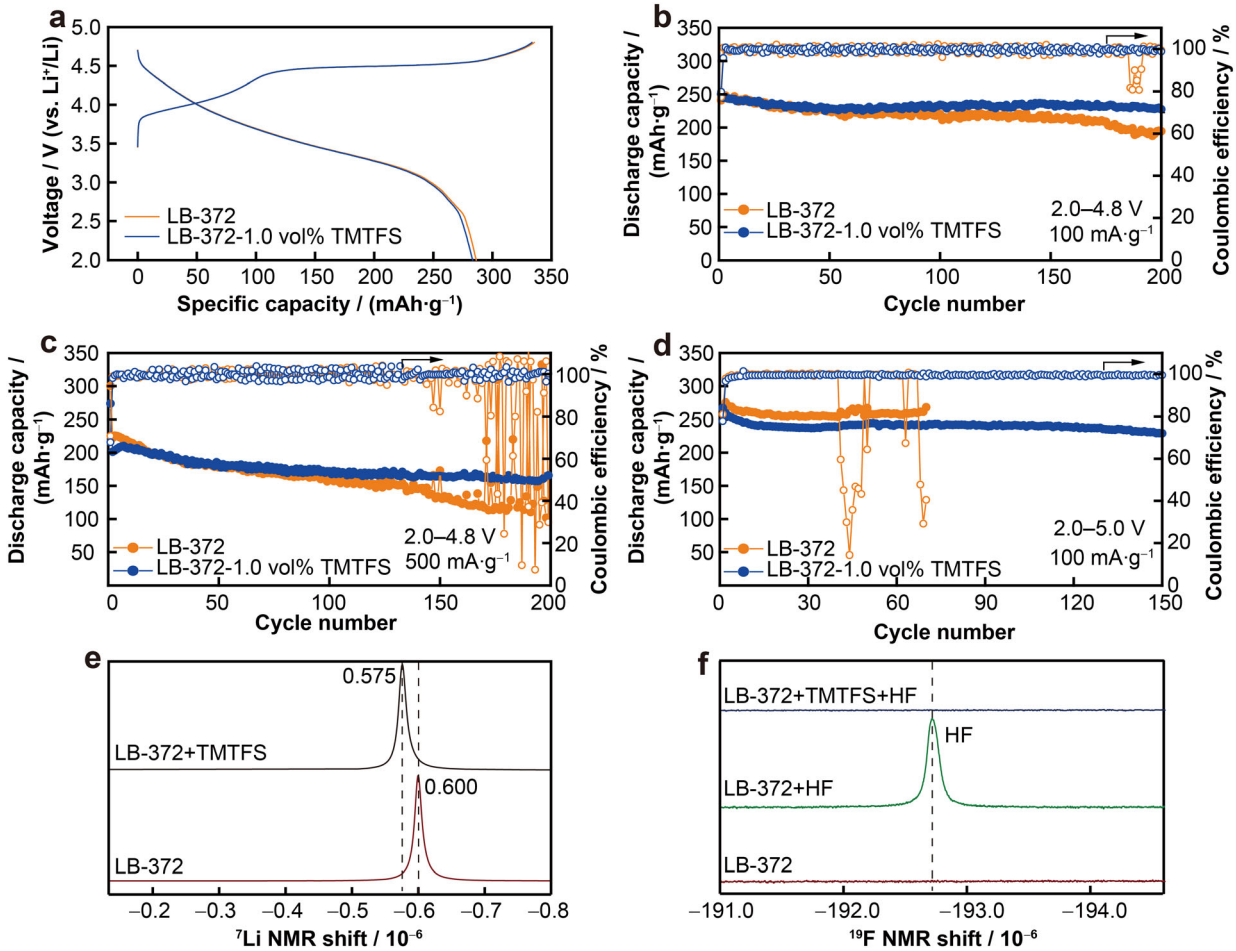

Fig. 2 **a** Initial charge–discharge profiles of LRMO electrode at 25 mA·g^{-1} in LB-372 and LB-372-1.0 vol% TMTFS electrolytes; cycling performance of LRMO cathodes at a current density of **b** 100 and **c** 500 mA·g^{-1} in LB-372 and LB-372-1.0 vol% TMTFS electrolytes between 2.0 and 4.8 V; **d** cycling performance of LRMO electrode at a current density of 100 mA·g^{-1} in LB-372 and LB-372-1.0 vol% TMTFS electrolytes between 2.0 and 5.0 V; **e** ^{7}Li NMR spectra of LB-372 and LB-372-1.0 vol% TMTFS electrolytes; **f** ^{19}F NMR spectra of LB-372 electrolyte and with HF or/and TMTFS

To elucidate the chemical component of the electrode/electrolyte interface, i.e., CEI layer, XPS was used to check the chemical bonding environments of the species. Figures 3c–f and S5 display the deconvolution of C 1s, F 1s and Si 2p XPS spectra of the samples after charge–discharge cycles. The deconvolution of the C 1s spectrum indicated that peaks of RO–CO_2Li/Li_2CO_3 (290.8 eV), C=O (287.9 eV), and C–O (286.2 eV) were attributed to the decomposed of solvent or additives [37, 47]. Compared to the reference peak (284.8 eV), the intensity of those three peaks is lower in the electrolyte with TMTFS than that of the electrolyte without additive (Fig. 3c, d). This result illustrated that this additive alleviated solvent decomposition. The F 1s XPS spectra indicated three species, i.e., C–F (687.9 eV), $Li_xPO_yF_z$ (687.2 eV) and LiF (685.3 eV), as shown in Fig. 3e, f. The intensity of the peak of $Li_xPO_yF_z$ is clearly decreased, but the peak of LiF is significantly increased when this additive is added into electrolyte. Combined to the deconvolution of the Si 2p spectrum (Fig. S5), it revealed that some of TMTFS was decomposed to construct the electrode/electrolyte interface, and formed a robust, thin, and dense LiF-dominated CEI layer, which is further confirmed by TEM images (Fig. 3) and EIS results (Fig. S6 and Table S1). Furthermore, SEM images showed that LRMO materials in LB-372-1.0 vol% TMTFS electrolyte contacted more tightly after 200 cycles (Fig. S7). It was worth noting that the clearly split diffraction peaks of (006), (012), (018) and (110) still existed in LB-372-1.0 vol% TMTFS electrolyte after cycles (Fig. S8). These results are believed that the TMTFS additive is to be the key factor in achieving the excellent cycling performance of LRMO electrode due to forming a unique CEI layer.

CV was employed to further assess the electrochemical performance of the electrode/electrolyte interface. The CV with various scan rates was recorded, as shown in Figs. 4,

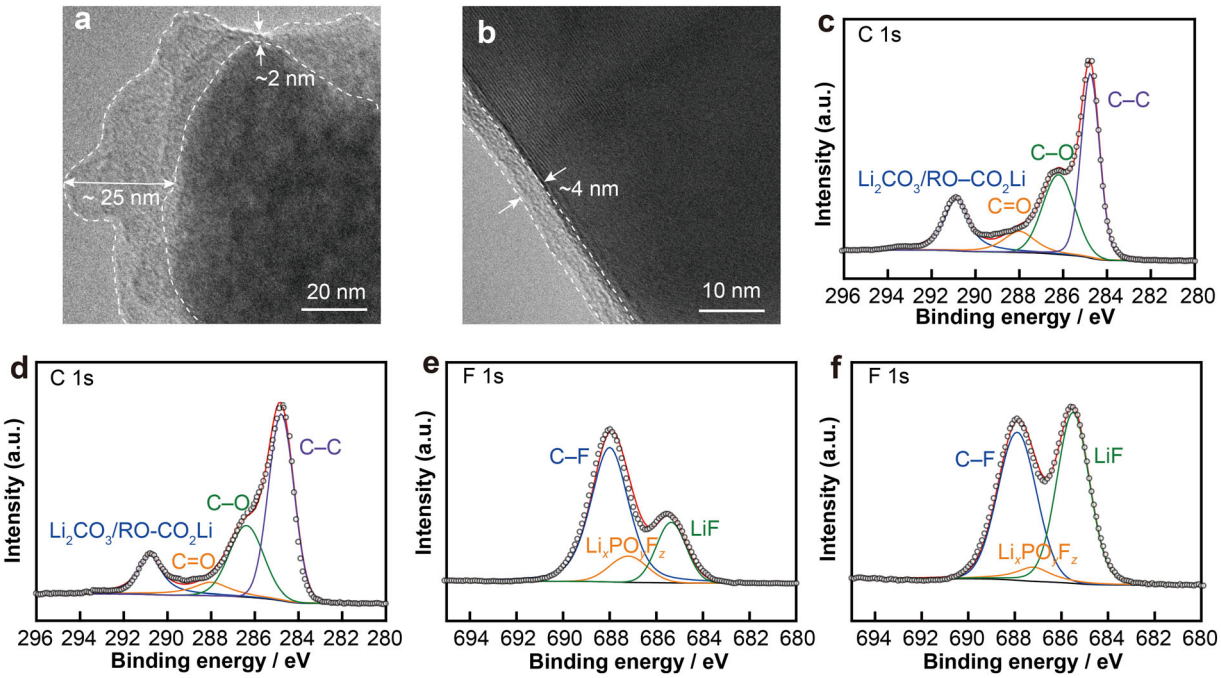

Fig. 3 TEM images of LRMO electrodes after cycling in **a** LB-372 and **b** LB-372-1.0 vol% TMTFS electrolytes; XPS spectra of LRMO electrodes after cycling in LB-372 (**c** and **e**) and LB-372-1.0 vol% TMTFS (**d** and **f**) electrolytes

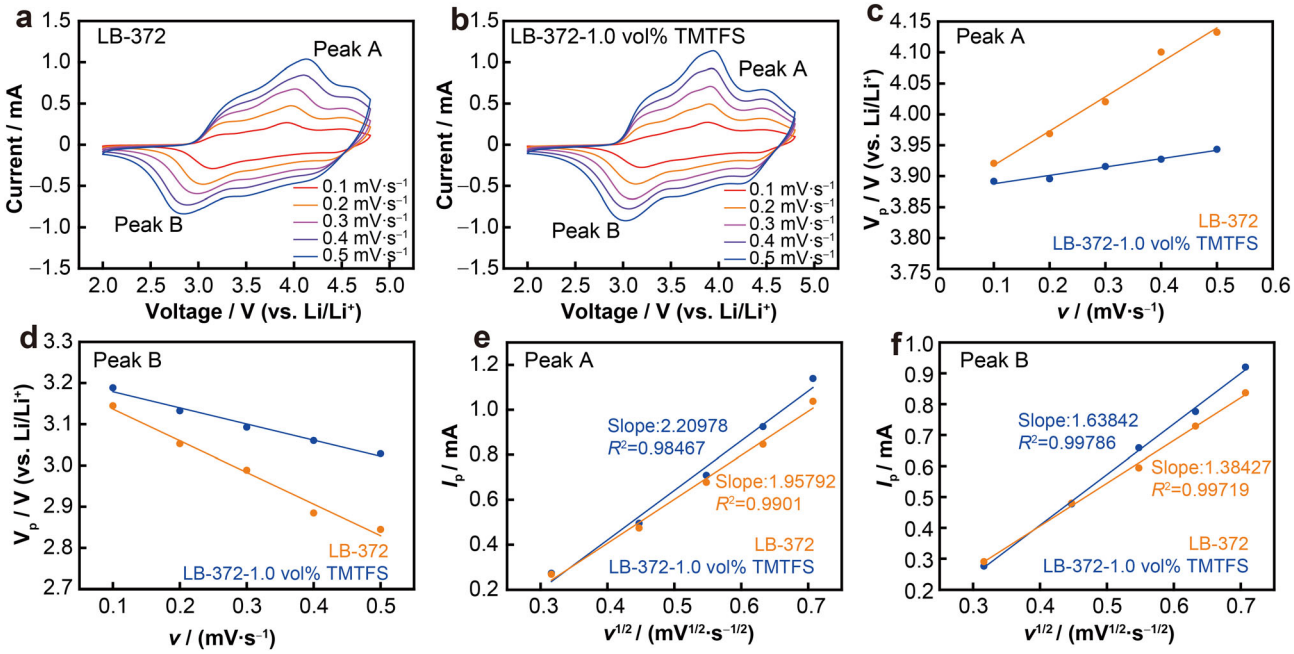

Fig. 4 CV curves of LRMO electrodes with different scanning rates: 0.1–0.5 mV·s^{-1} in **a** LB-372 and **b** LB-372-1.0 vol% TMTFS electrolytes, and corresponding relationship between **c, d** V_p and v, **e, f** I_p and $v^{1/2}$

S9. When the scan rate increased from 0.1 to 0.5 mV·s^{-1}, the anodic peak (A) shifted by 212 and 52 mV to higher potentials, while the cathodic peak (B) shifted by 300 and 160 mV to lower potentials for electrolyte without/with the TMTFS additive, respectively. Obviously, there is a larger polarization in electrolyte without the additive, which can be further supported by TEM images (Fig. 3). We calculated the apparent lithium-ion diffusion coefficients, which reflects the kinetics of lithium insertion/extraction at the electrode/electrolyte interface (Fig. 4e, f), according to the classical Randles–Sevcik equation [48]. Clearly, all the apparent lithium-ion diffusion coefficients of the battery

with the TMTFS additive are larger than that of battery without this additive (Table S2). This difference value of the diffusion rates and polarization can be attributed to the structure and component of the electrode/electrolyte interface, which was improved by the TMTFS additive. This result is further supported by the excellent cycling performance of the LRMO electrodes with the TMTFS additive.

We carried out in situ PXRD studies of the LRMO electrode to check the structure changes during the first three cycles under the current density of 25 $mA{\cdot}g^{-1}$. The contour map of in situ PXRD and the corresponding charge–discharge profiles are displayed in Figs. 5, S10. The unshifted peaks are attributable to current collector, beryllium window, and the device of the in situ cell. During the first charging process, some peaks, including (003) and (018), shift to lower angle at first, then keep a period of time, and then a little back to higher angle. It is attributed that lithium ions are extracted from lithium layers and transition metal layers with different structure changes, resulting in *c*-parameter increasing at first, then keeping constant, and then decreasing later [49]. With extraction of lithium from the lithium layers, the electrostatic repulsion between oxygen layers induced the increase of *c*-parameter. With further extraction of lithium to ~ 4.5 V, the lithium of transition metal layers was activated and entered into the lithium layers, which kept the *c*-parameter constant during this process. When the speed of extraction lithium is larger than that of lithium from transition metal layers entered into lithium layers, the lithium lays contracted, meanwhile, oxygen released and transition metal entered into the lithium layers, which may decrease the electrostatic repulsion and then decrease the *c*-parameter [49]. Other peaks shifted to higher angle, which is related to *a*-parameter [50]. During the initial discharge process, the lithium ions also have two processes, i.e., insertion into lithium layers and transition metal layers, resulting in the peaks shifted to inverse direction of the charging process. During subsequent two cycles, similar phenomena were observed. The periodic shift of the peaks indicated a reversible lithiation/delithiation process. It should be noted that the positions of (003) and (018) peaks at full charge and full discharge stages are almost constant, which is related to the change of *c*-parameter. This phenomenon observed by in situ PXRD is similar to previous reports [49–51].

In summary, we report TMTFS as a new multifunctional electrolyte additive, which significantly enhance the cycling stability of the $Li_{1.2}Ni_{0.13}Co_{0.13}Mn_{0.54}O_2$ cathode. A LRMO electrode delivered a reversible capacity about 227.6 and 195.8 $mAh{\cdot}g^{-1}$ at 0.4C and 1.0C after 200 cycles with a capacity retention of 91% and 81%,

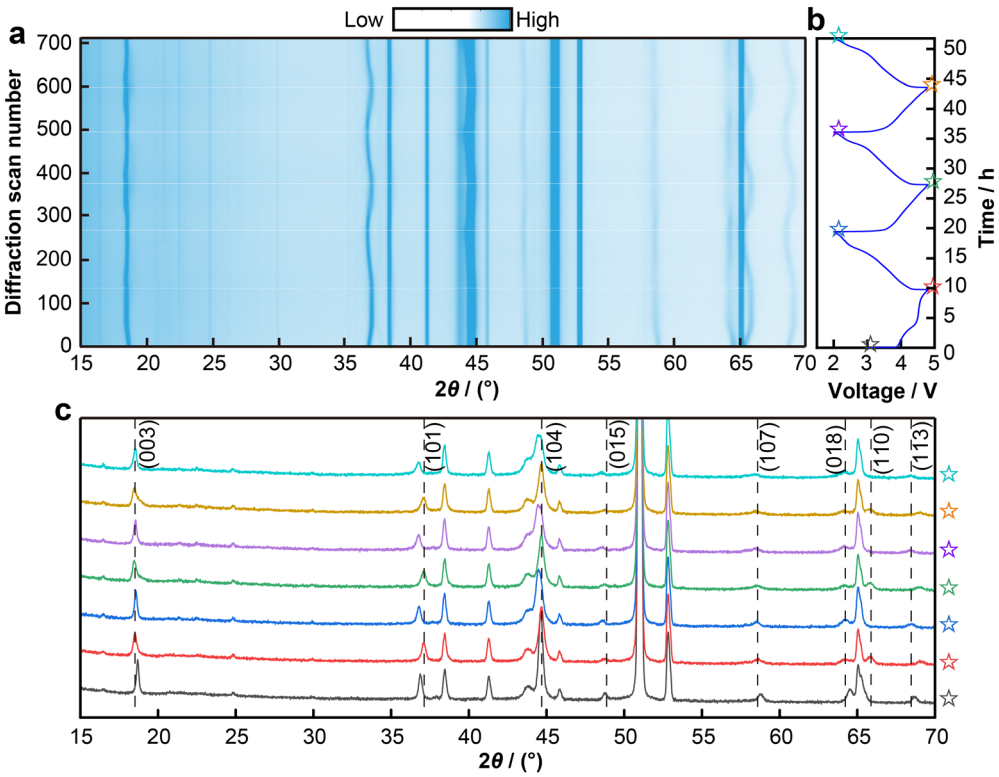

Fig. 5 **a**, **b** First three-cycles curves and corresponding in situ PXRD patterns of LRMO electrode in LB-372-1.0 vol% TMTFS electrolyte at 25 $mA{\cdot}g^{-1}$; **c** discrete PXRD patterns selected from Panel **a**

respectively, compared to those (only 77% and 46%) in electrolyte without TMTFS under the same conditions. ^{7}Li and ^{19}F NMR spectra revealed that the TMTFS additive can change the structure of electrolyte, the solvation environment of lithium ions and HF scavenging. XPS, TEM, EIS and CV results confirmed that the TMTFS additive can promote a robust, thin, and dense LiF-dominated cathode electrolyte interphase on the LRMO cathode. From this study, a fundamental understanding of the function of TMTFS additive can serve as a guide for designing new additives for Li-rich layered oxide cathode materials.

Acknowledgments This study was financially supported by the National Natural Science Foundation of China (Nos. 22172116 and 21773176). We thank Prof. Hexiang Deng and Jin Liu (Wuhan University) for their invaluable assistance. F.S.K. acknowledges the Large-scale Instrument and Equipment Sharing Foundation of Wuhan University.

Declarations

Conflict of interests The authors declare that they have no conflict of interest.

References

[1] Yang HL, Zhang BW, Wang YX, Konstantinov K, Liu HK, Dou SX. Alkali-metal sulfide as cathodes toward safe and high-capacity metal (M = Li, Na, K) sulfur batteries. Adv Energy Mater. 2020;10(37):2001764. https://doi.org/10.1002/aenm.202001764.

[2] Deng D. Li-ion batteries: basics, progress, and challenges. Energy Sci Eng. 2015;3(5):358. https://doi.org/10.1002/ese3.95.

[3] Ke CZ, Liu F, Zheng ZM, Zhang HH, Zhang QB. Boosting lithium storage performance of Si nanoparticles via thin carbon and nitrogen/phosphorus co-doped two-dimensional carbon sheet dual encapsulation. Rare Met. 2021;40(6):1347. https://doi.org/10.1007/s12598-021-01716-1.

[4] Feng XY, Wu HH, Gao B, Świętosławski M, He X, Zhang QB. Lithiophilic N-doped carbon bowls induced Li deposition in layered graphene film for advanced lithium metal batteries. Nano Res. 2022;15(1):352. https://doi.org/10.1007/s12274-021-3482-0.

[5] Bayaguud A, Zhang Z, Geng M, Fu Y, Zhu C. Transformation of polyoxometalate into 3D porous Li-containing oxide: a case study of gamma-LiV_2O_5 for high-performance cathodes of Li-ion batteries. Small Method. 2019;3:1900187. https://doi.org/10.1002/smtd.201900187.

[6] Kim T, Song WT, Son DY, Ono LK, Qi YB. Lithium-ion batteries: outlook on present, future, and hybridized technologies. J Mater Chem A. 2019;7:2942. https://doi.org/10.1039/C8TA10513H.

[7] Li X, Jiang YZ, Li XK, Jiang HX, Liu JL, Feng J. Electrochemical property of $LiFePO_4$/C composite cathode with different carbon sources. Rare Met. 2018;37(9):743. https://doi.org/10.1007/s12598-016-0781-9.

[8] Gu XX, Qiao S, Ren XL, Liu XY, He YZ, Liu XT, Liu TF. Multi-core-shell-structured $LiFePO_4@Na_3V_2(PO_4)_3$@C composite for enhanced low-temperature performance of lithium-ion batteries. Rare Met. 2021;40(4):828. https://doi.org/10.1007/s12598-020-01669-x.

[9] Nitta N, Wu FX, Lee JT, Yushin G. Li-ion battery materials: present and future. Mater Today. 2015;18(5):252. https://doi.org/10.1016/j.mattod.2014.10.040.

[10] Wu F, Maier J, Yu Y. Guidelines and trends for next-generation rechargeable lithium and lithium-ion batteries. Chem Soc Rev. 2020;49(5):1569. https://doi.org/10.1039/C7CS00863E.

[11] Zhou DYY, Guo XT, Zhang QY, Shi YX, Zhang HB, Yu C, Pang H. Nickel-based materials for advanced rechargeable batteries. Adv Funct Mater. 2022;32(12):2107928. https://doi.org/10.1002/adfm.202107928.

[12] Huang C, Wang ZJ, Fang ZQ, Zhao SX, Ci LJ. Achieving high initial coulombic efficiency and low voltage dropping in Li-rich Mn-based cathode materials by metal-organic frameworks-derived coating. J Power Sources. 2021;499: 229967. https://doi.org/10.1016/j.jpowsour.2021.229967.

[13] Wang Z, Lu HQ, Yin YP, Sun XY, Bai XT, Shen XL, Zhuang WD, Lu SG. $FePO_4$-coated $Li[Li_{0.2}Ni_{0.13}Co_{0.13}Mn_{0.54}]O_2$ with improved cycling performance as cathode material for Li-ion batteries. Rare Met. 2017;36(11):899. https://doi.org/10.1007/s12598-015-0647-6.

[14] Li HM, Guo HJ, Wang ZX, Wang JX, Li XH, Chen N, Gui WH. Improving rate capability and decelerating voltage decay of Li-rich layered oxide cathodes by chromium doping. Int J Hydrog Energy. 2018;43(24):11109. https://doi.org/10.1016/j.ijhydene.2018.04.203.

[15] Zhang K, Qi JZ, Song J, Zuo YX, Yang YL, Yang TH, Chen T, Liu X, Chen LW, Xia DJ. Sulfuration of Li-rich Mn-based cathode materials for multianionic redox and stabilized coordination environment. Adv Mater. 2022;34(11):2109564. https://doi.org/10.1002/adma.202109564.

[16] Sun YK, Lee MJ, Yoon CS, Hassoun J, Amine K, Scrosati B. T the role of AlF_3 coatings in improving electrochemical cycling of Li-enriched nickel-manganese oxide electrodes for Li-ion batteries. Adv Mater. 2012;24(9):1192. https://doi.org/10.1002/adma.201104106.

[17] Yang JS, Li P, Zhong FP, Feng XM, Chen WH, Ai XP, Yang HX, Xia DG, Cao YL. Suppressing voltage fading of Li-rich oxide cathode via building a well-protected and partially-protonated surface by polyacrylic acid binder for cycle-stable li-ion batteries. Adv Energy Mater. 2020;10(15):1904264. https://doi.org/10.1002/aenm.201904264.

[18] Sathiya M, Abakumov AM, Foix D, Rousse G, Ramesha K, Saubanère M, Doublet ML, Vezin H, Laisa CP, Prakash AS, Gonbeau D, Tendeloo GV, Tarascon JM. Origin of voltage decay in high-capacity layered oxide electrodes. Nat Mater. 2015;14(2):230. https://doi.org/10.1038/nmat4137.

[19] Yu HL, Belay Ibrahim K, Chi PW, Su YH, Chen WT, Tseng SC, Tang MT, Chen CL, Tang HY, Pao CW, Chen KH, Wu MK, Wu HL. Modulating the voltage decay and cationic redox kinetics of Li-rich cathodes via controlling the local electronic structure. Adv Funct Mater. 2022. https://doi.org/10.1002/adfm.202112394.

[20] Hwang J, Myeong S, Lee E, Jang H, Yoon M, Cha H, Sung J, Kim MG, Seo DH, Cho J. Lattice-oxygen-stabilized Li- and Mn-rich cathodes with sub-micrometer particles by modifying the excess-Li distribution. Adv Mater. 2021;33(18):2100352. https://doi.org/10.1002/adma.202100352.

[21] Ahn J, Kang J, Cho MK, Park H, Ko W, Lee Y, Kim HS, Jung YH, Jeon TY, Kim H, Ryu WH, Hong J, Kim J. Selective anionic redox and suppressed structural disordering enabling high-energy and long-life Li-rich layered-oxide cathode. Adv Energy Mater. 2021;11(47):2102311. https://doi.org/10.1002/aenm.202102311.

[22] Fu CC, Meng LL, Wang JF, Wang Q, Yang K, Zhang WM, Li LP. Bonding the terminal isocyanate-related functional group to the surface manganese ions to enhance Li-rich cathode's cycling

stability. ACS Appl Mater Interfaces. 2021;13(15):17565. https://doi.org/10.1021/acsami.1c01726.
[23] Jiang B, Li JR, Luo B, Yan QZ, Li H, Liu LH, Chu LH, Li YF, Zhang QB, Li MC. $LiPO_2F_2$ electrolyte additive for high-performance Li-rich cathode material. J Energy Chem. 2021;60:564. https://doi.org/10.1016/j.jechem.2021.01.024.
[24] Su YF, Yuan FY, Chen L, Lu Y, Dong JY, Fang YY, Chen S, Wu F. Enhanced high-temperature performance of Li-rich layered oxide via surface heterophase coating. J Energy Chem. 2020;51:39. https://doi.org/10.1016/j.jechem.2020.03.033.
[25] Luo Q, Xie YX, Wu ZJ, Xie Q, Yan D, Zou HB, Yang W, Chen SZ. Facile molten vanadate-assisted surface treatment strategy for Li_2MnO_3 activation of Li-rich cathode materials. ACS Appl Energy Mater. 2021;4(5):4867. https://doi.org/10.1021/acsaem.1c00453.
[26] Seaby T, Lin TE, Hu YX, Yuan QH, Wang LZ. An analysis of F-doping in Li-rich cathodes. Rare Met. 2022;41(6):1771. https://doi.org/10.1007/s12598-021-01883-1.
[27] Liu T, Zhao SX, Gou LL, Wu X, Nan CW. Electrochemical performance of Li-rich cathode material, $0.3Li_2MnO_3$–$0.7LiMn_{1/3}Ni_{1/3}Co_{1/3}O_2$ microspheres with F-doping. Rare Met. 2019;38(3):189. https://doi.org/10.1007/s12598-018-1168-x.
[28] Fan QL, Yang SD, Liu J, Liu HD, Lin KJ, Liu R, Hong CY, Liu LY, Chen Y, An K, Liu P, Shi ZC, Yang Y. Mixed-conducting interlayer boosting the electrochemical performance of Ni-rich layered oxide cathode materials for lithium ion batteries. J Power Sources. 2019;421:91. https://doi.org/10.1016/j.jpowsour.2019.03.014.
[29] Yang SD, Fan QL, Shi ZC, Liu LY, Liu J, Ke X, Liu JP, Hong CY, Yang Y, Guo ZP. Superior stability secured by a four-phase cathode electrolyte interface on a Ni-rich cathode for lithium ion batteries. ACS Appl Mater Interfaces. 2019;11(40):36742. https://doi.org/10.1021/acsami.9b12578.
[30] Fan QL, Lin KJ, Shi ZC, Guan SJ, Chen JB, Feng S, Liu LY. Constructing high conductive composite coating with TiN and polypyrrole to improve the performance of $LiNi_{0.8}Co_{0.1}Mn_{0.1}O_2$ at high cutoff voltage of 4.5 V. ACS Appl. Energy Mater. 2021;4(9):10012. https://doi.org/10.1021/acsaem.1c01934.
[31] Huang ZX, Li GZ, Huang YL, Gu XF, Wang NG, Liu JP, Li OL, Shao HY, Yang Y, Shi ZC. Facile one-pot synthesis of low cost MnO_2 nanosheet/Super P Li composites with high oxygen reduction reaction activity for Zn-air batteries. J Power Sources. 2020;448: 227385. https://doi.org/10.1016/j.jpowsour.2019.227385.
[32] Wynn TA, Fang CC, Zhang MH, Liu HD, Davies DM, Wang XF, Lau D, Lee JZ, Huang BY, Fung KZ, Ni CT, Meng YS. Mitigating oxygen release in anionic-redox-active cathode materials by cationic substitution through rational design. J Mater Chem A. 2018;6(47):24651. https://doi.org/10.1039/C8TA06296J.
[33] Wu F, Li WK, Chen L, Lu Y, Su YF, Bao W, Wang J, Chen S, Bao LY. Polyacrylonitrile-polyvinylidene fluoride as high-performance composite binder for layered Li-rich oxides. J Power Sources. 2017;359:226. https://doi.org/10.1016/j.jpowsour.2017.05.063.
[34] Zhang GH, Qiu B, Xia YG, Wang XL, Gu QW, Jiang YB, He ZL, Liu ZP. Advanced double-helix-superstructure aqueous binder to boost excellent electrochemical performance in Li-rich layered oxide cathode. J Power Sources. 2019;420:29. https://doi.org/10.1016/j.jpowsour.2019.02.086.
[35] Zhang SM, Gu HT, Pan HG, Yang SH, Du WB, Li X, Gao MX, Liu YF, Zhu M, Ouyang LZ, Jian DC, Pan F. A novel strategy to suppress capacity and voltage fading of Li- and Mn-rich layered oxide cathode material for lithium-ion batteries. Adv Energy Mater. 2017;7(6):1601066. https://doi.org/10.1002/aenm.201601066.
[36] Wang L, Ma YL, Li Q, Zhou ZX, Cheng XQ, Zuo PJ, Du CY. Gao YZ, Yin GP. 1,3,6-hexanetricarbonitrile as electrolyte additive for enhancing electrochemical performance of high voltage Li-rich layered oxide cathode. Journal of Power Sources. 2017;361:227. https://doi.org/10.1016/j.jpowsour.2017.06.075.
[37] Deng T, Fan XL, Cao LS, Chen J, Hou S, Ji X, Chen L, Li S, Zhou XQ, Hu EY, Su D, Yang XQ, Wang CS. Designing in-situ-formed interphases enables highly reversible cobalt-free $LiNiO_2$ cathode for Li-ion and Li-metal batteries. Joule. 2019;3(10):2550. https://doi.org/10.1016/j.joule.2019.08.004.
[38] Yu ZA, Wang HS, Kong X, Huang W, Tsao Y, Mackanic DG, Wang KC, Wang XC, Huang WX, Choudhury S, Zheng Y, Amanchukwu CV, Hung ST, Ma YT, Lomeli EG, Qin J, Cui Y, Bao ZN. Molecular design for electrolyte solvents enabling energy-dense and long-cycling lithium metal batteries. Nat Energy. 2020;5(7):526. https://doi.org/10.1038/s41560-020-0634-5.
[39] Li YX, Li WK, Shimizu R, Cheng DY, Nguyen HN, Paulsen J, Kumakura S, Zhang MH, Meng YS. Elucidating the effect of borate additive in high-voltage electrolyte for Li-rich layered oxide materials. Adv Energy Mater. 2022;12(11):2103033. https://doi.org/10.1002/aenm.202103033.
[40] He W, Qian JF, Cao YL, Ai XP, Yang HX. Improved electrochemical performances of nanocrystalline $Li[Li_{0.2}Mn_{0.54}Ni_{0.13}Co_{0.13}]O_2$ cathode material for Li-ion batteries. RSC Advances. 2012;2(8):3423. https://doi.org/10.1039/C2RA20122D.
[41] Yu LH, Cao YL, Yang HX, Ai XP. Synthesis and electrochemical properties of high-voltage $LiNi_{0.5}Mn_{1.5}O_4$ electrode material for Li-ion batteries by the polymer-pyrolysis method. J Solid State Electrochem. 2006;10:283. https://doi.org/10.1007/s10008-005-0695-1.
[42] Xiao Lf, Yang YY, Zhao YQ, Ai XP, Yang HX, Cao YL. Synthesis and electrochemical properties of submicron $LiNi_{0.8}Co_{0.2}O_2$ by a polymer-pyrolysis method. Electrochim. Acta. 2008;53(6):3007. https://doi.org/10.1016/j.electacta.2007.11.013.
[43] Thackeray MM, Kang SH. Johnson CS, Vaughey JT, Hackney SA. Comments on the structural complexity of lithium-rich $Li_{1+x}M_{1-x}O_2$ electrodes (M = Mn, Ni, Co) for lithium batteries. Electrochem. Commun. 2006;8(9):1531. https://doi.org/10.1016/j.elecom.2006.06.030.
[44] Hu YM, Dunlap N, Wan S, Lu SL, Huang SF, Sellinger I, Ortiz M, Jin YH, Lee SH, Zhang W. Crystalline lithium imidazolate covalent organic frameworks with high Li-ion conductivity. J Am Chem Soc. 2019;141(18):7518. https://doi.org/10.1021/jacs.9b02448.
[45] Zhang LH, Min FQ, Luo Y, Dang GJ, Gu HT, Dong QY, Zhang MH, Sheng LM, Shen YB, Chen LW, Xie JY. Practical 4.4 V Li‖NCM811 batteries enabled by a thermal stable and HF free carbonate-based electrolyte. Nano Energy. 2022;96:107122. https://doi.org/10.1016/j.nanoen.2022.107122.
[46] Zheng YZ, Xu NB, Chen SJ, Liao Y, Zhong GM, Zhang ZR, Yang Y. Construction of a stable $LiNi_{0.8}Co_{0.1}Mn_{0.1}O_2$ (NCM811) cathode interface by a multifunctional organosilicon electrolyte additive. ACS Appl. Energy Mater. 2020;3(3):2837. https://doi.org/10.1021/acsaem.9b02486.
[47] Ye CC, Tu WQ, Yin LM, Zheng QF, Wang C, Zhong YT, Zhang YG, Huang QM, Xu K, Li WS. Converting detrimental HF in electrolytes into a highly fluorinated interphase on cathodes. J Mater Chem A. 2018;6(36):17642. https://doi.org/10.1039/C8TA06150E.
[48] Ke FS, Huang L, Jamison L, Xue LJ, Guo ZW, Li JT, Zhou XD, Sun SG. Nanoscale tin-based intermetallic electrodes encapsulated in microporous copper substrate as the negative electrode with a high rate capacity and a long cycleability for lithium-ion batteries. Nano Energy. 2013;2(5):595. https://doi.org/10.1016/j.nanoen.2013.06.004.

[49] Mohanty D, Kalnaus S, Meisner RA, Rhodes KJ, Li JL, Payzant EA, Wood DL, Daniel C. Structural transformation of a lithium-rich $Li_{1.2}Co_{0.1}Mn_{0.55}Ni_{0.15}O_2$ cathode during high voltage cycling resolved by in situ X-ray diffraction. J. Power Sources. 2013;229:239. https://doi.org/10.1016/j.jpowsour.2012.11.144.

[50] Shen SY, Hong YH, Zhu FC, Cao ZM, Li YY, Ke FS, Fan JJ, Zhou LL, Wu LN, Dai P, Cai MZ, Huang L, Zhou ZY, Li JT, Wu QH, Sun SG. Tuning electrochemical properties of Li-rich layered oxide cathodes by adjusting Co/Ni ratios and mechanism investigation using in situ X-ray diffraction and online continuous flow differential electrochemical mass spectrometry. ACS Appl Mater Interfaces. 2018;10(15):12666. https://doi.org/10.1021/acsami.8b00919.

[51] Chernyavsky V, Kim A, Koshtyal Y, Rumyantsev A, Popovich A, Maximov MY. Structural features of complete and partial activation of Li-rich cathodes studied by in-situ XRD. Electrochim Acta. 2022;414: 140237. https://doi.org/10.1016/j.electacta.2022.140237.